Orientation and shape of flexible polymers in a slit

van Vliet, J. H.; ten Brinke, G.

Published in:
Journal of Chemical Physics

DOI:
10.1063/1.459153

Orientation and shape of flexible polymers in a slit

J. H. van Vliet and G. ten Brinke
Department of Polymer Chemistry, University of Groningen, Groningen, The Netherlands

(Received 17 January 1990; accepted 2 April 1990)

The shape and orientation of a polymer in a good solvent confined between two parallel plates is investigated by Monte Carlo simulations of self-avoiding random walks on a simple cubic lattice. Decreasing the width of the slit, the coil starts, due to its anisotropic shape, to orient long before its shape changes. Only after the longest principal axis is aligned considerably parallel to the plates, the coil is squeezed. Using a scaled distance between the plates, a corresponding state behavior as a function of chain length is found. The results are in good agreement with predictions based on an analytical rigid ellipsoid model with principal axes' lengths set equal to the span lengths along the principal axes of inertia of the self-avoiding random walk.

INTRODUCTION

The asymmetric shape of a polymer coil was first recognized by Kuhn.[1] An appropriate way to discuss the shape is by means of inertial properties; the shape of each conformation being described in terms of the three principal components of the radius of gyration.[2-4] The shape distribution for Gaussian molecules was studied by Eichinger.[5-7] His approach clearly shows that entropy forces the distribution function to be anisotropic. Basically, the number of ellipsoidal conformations far outnumbers the number of spherical conformations. These remarks are not restricted to Gaussian statistics, i.e., θ-conditions, but hold equally well for a dilute solution of polymers in a good solvent, which theoretically corresponds to self-avoiding random walk or excluded volume statistics. Numerical calculations of polymer chains with excluded volume were first performed by Mazur *et al.*[8] and excluded volume chains were shown to be even more anisotropic than nonexcluded volume chains.

The anisotropy of polymer coils shows up in a variety of problems like polymer-induced fluctuations in high strain rate laminar flows,[9] smooth-density theories of dilute solution properties of chain molecules,[10] and maybe even in the orientation of flexible polymers in nematic solvents.[11-13] In most practical situations, the effect of the instantaneous high asymmetry of chain molecules is restricted to time scales, short compared to the longest relaxation time of the coil.[14,15] In anisotropic environments, such as slit-like pores, this is no longer the case.

In a series of papers, Wall *et al.*[16-18] reported the results of numerical calculations of self-avoiding random walks (SAW's) confined to a slit. In these studies, the component of the radius of gyration parallel to the plates was considered, and the results were in a subsequent paper[19] compared with scaling predictions of Daoud and De Gennes.[20] Since scaling predictions are based on the assumption of the existence of one characteristic length, the so-called Flory radius, this kind of approach fails to detect the effect of confinement on the orientation and shape of highly anisotropic objects like polymer coils. In the present study, the influence of confinement on polymer molecules in a dilute good solvent is considered in more detail.

The shape and orientation of a polymer coil is characterized by the eigenvalues and eigenvectors of the radius of gyration matrix. In descending order, the eigenvalues are denoted by λ_1, λ_2, and λ_3. They are related to the mean-square radius of gyration $\langle S^2 \rangle$ by

$$\langle S^2 \rangle = \langle \lambda_1 \rangle + \langle \lambda_2 \rangle + \langle \lambda_3 \rangle, \tag{1}$$

where $\langle\ \rangle$ indicates an average over all conformations. In three-dimensional space, the square roots of these eigenvalues can be pictured as half the lengths of the principal axes of an ellipsoid. To study the effect of the width of the slit L on the orientation, and shape of a polymer coil in a dilute good solvent, $\langle \lambda_1 \rangle$, $\langle \lambda_2 \rangle$, and $\langle \lambda_3 \rangle$ are used to characterize the shape and the orientation functions $\langle \cos^2 \alpha \rangle$, $\langle \cos^2 \beta \rangle$, and $\langle \cos^2 \gamma \rangle$, angles with the direction perpendicular to the plates, to characterize the orientation of the corresponding principal axes. To calculate these quantities, Monte Carlo simulations of self-avoiding walks on a simple cubic lattice were performed. A representative statistical sample was generated by the "slithering snake" or "reptation" algorithm.[21,22] The results are compared with predictions based on an analytical ellipsoidal solid body confined to a slit. Good agreement is found by taking the lengths of the three principal axes of this solid body equal to the span lengths along the principal axes of the corresponding SAW's. A corresponding state behavior for different chain lengths is found by using a scaled distance between the plates.

METHOD

Monte Carlo simulations of a SAW on a simple cubic lattice with periodical boundary conditions in the X and Y directions were performed. The two parallel plates were perpendicular to the Z axis. The length of the lattice in the X and Y directions depended on the number of steps of the SAW considered. In all cases, this length exceeded the mean-square end-to-end point distance of the SAW. The number of steps of the SAW's considered were $N = 39$, 79, 159, 319, and 639, respectively. For each chain length considered, the lattice length in the X and Y directions was fixed and the distance between the plates varied. For the shortest distance between the plates considered, the densities, expressed as the

 0021-9606/90/141436-06$03.00

fraction of lattice sites occupied, varied between 16.5% for $N = 39$ to 0.52% for $N = 639$. For greater distances between the plates, the density was correspondingly lower. For each chain length and distance between the plates, a representative sample was obtained by the reptation algorithm.[21,22] To speed up equilibration, chain growth and reptation took place simultaneously. The first 2×10^6 attempted moves after completion of chain growth were ignored. From the subsequent interval of 2×10^6 attempted moves 17 times, at equally spaced intervals, quantities of interest were calculated and averaged afterwards. This procedure was repeated for five independent runs. After averaging again, the statistical errors were calculated as usual from the averages per run.

RESULTS AND DISCUSSION

Characteristic lengths of SAW's in three dimensions, like the mean-square radius of gyration $\langle S^2\rangle$, are known to scale with chain length N as

$$\langle S^2\rangle \sim N^{2\nu}, \tag{2}$$

where ν is approximately equal to 0.6[23,24] The most accurate value available to date for a simple cubic lattice is 0.592.[25,26] Furthermore, for not too small N, the ratio between the mean-square principal radii of gyration satisfies[8]

$$\langle\lambda_1\rangle:\langle\lambda_2\rangle:\langle\lambda_3\rangle = 14.8:3.06:1. \tag{3}$$

Equations 1 and 3 together imply

$$\langle\lambda_1\rangle = 0.785\langle S^2\rangle,$$
$$\langle\lambda_2\rangle = 0.162\langle S^2\rangle, \quad \text{and} \quad \langle\lambda_3\rangle = 0.053\langle S^2\rangle. \tag{4}$$

Clearly $\langle\lambda_1\rangle$, $\langle\lambda_2\rangle$, and $\langle\lambda_3\rangle$ also satisfy the scaling relation given by Eq. (2). Therefore, in order to compare results for different values of N, the distance between the plates is expressed in units Δ defined by

$$\Delta \equiv L/N^{0.592}. \tag{5}$$

The influence of the confinement is discussed in terms of $\langle S^2\rangle/\langle S^2\rangle_0$, $\langle\lambda_i\rangle/\langle\lambda_i\rangle_0$, with $i = 1, 2, 3$, and $\langle\cos^2\alpha\rangle$, $\langle\cos^2\beta\rangle$ and $\langle\cos^2\gamma\rangle$. Here, the index zero indicates the unconfined SAW. The values for the mean-square radius of gyration of the unconfined SAW on a simple cubic lattice were taken from Rapaport's paper.[25] The corresponding values for the squares of the principal radii of gyration are then found from Eq. (4).

Figure 1 shows $\langle S^2\rangle/\langle S^2\rangle_0$, as a function of Δ. For Δ exceeding 1.5, a nearly constant value slightly smaller than one is reached. This small deviation is due to the fact that a small fraction of all conformations has its center of mass within such a distance to one of the plates that deformation is unavoidable. For $\Delta\to\infty$, the limiting values of one will obviously be reached. For Δ smaller than 1.5, the mean-square radius of gyration first decreases which, as will become clear further on, corresponds to a slight compression of the coil. For values of Δ smaller than one, $\langle S^2\rangle$ increases again until it reaches its final two-dimensional value. As will be shown, $\Delta = 1$ corresponds approximately to the distance between the plates for which the value of the smallest mean-square principal radius of gyration $\langle\lambda_3\rangle$ starts to decrease from the unconfined value. From that moment on, the polymer coil is really squeezed and the corresponding increase in excluded volume interaction forces $\langle S^2\rangle$ to increase.

Figures 2–4 show $\langle\lambda_i\rangle/\langle\lambda_i\rangle_0$ as a function of Δ. The largest principal component remains nearly constant for $\Delta \geqslant 1.5$, then decreases slightly and finally increases again for $\Delta \leqslant 1$, until it reaches the limiting two-dimensional value. This behavior is not unlike that of the mean-square radius of gyration discussed before. The second largest principal component behaves similarly, although the deviation from the plateau value occurs at a slightly smaller value of Δ. The smallest principal component, finally, remains constant for $\Delta \geqslant 1$. For smaller distances between the plates, it gradually decreases towards the limiting value of zero. Before we dis-

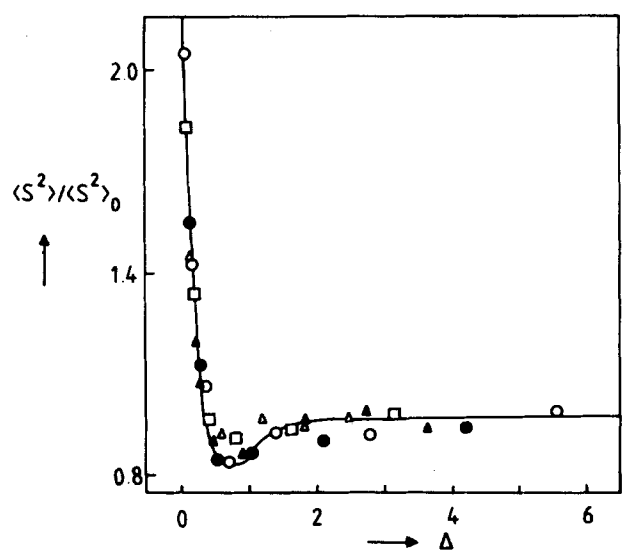

FIG. 1. $\langle S^2\rangle/\langle S^2\rangle_0$ as a function of Δ. ▲:$N = 39$, △:$N = 79$, □:$N = 159$, ●:$N = 319$, ○:$N = 639$; maximum error is 0.12 for all N.

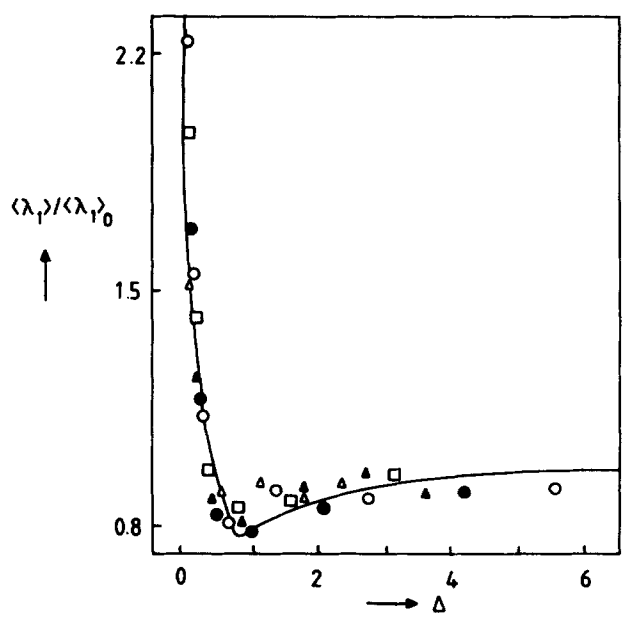

FIG. 2. $\langle\lambda_1\rangle/\langle\lambda_1\rangle_0$ as a function of Δ. ▲:$N = 39$, △:$N = 79$, □:$N = 159$, ●:$N = 319$, ○:$N = 639$; maximum error increases from 0.09 for $N = 39$ to 0.20 for $N = 639$.

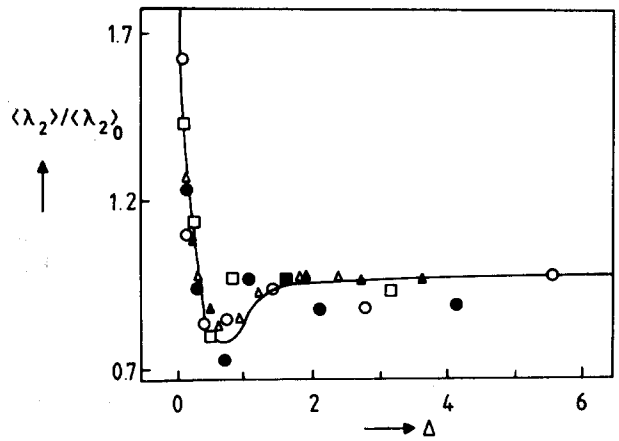

FIG. 3. $\langle\lambda_2\rangle/\langle\lambda_2\rangle_0$ as a function of Δ. ▲:$N=39$, △:$N=79$, □:$N=159$, ●:$N=319$, ○:$N=639$; maximum error increases from 0.07 for $N=39$ to 0.14 for $N=639$.

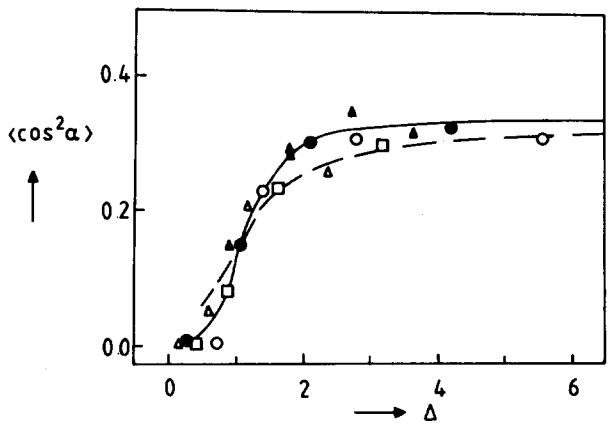

FIG. 5. $\langle\cos^2\alpha\rangle$ as a function of Δ. ▲:$N=39$, △:$N=79$, □:$N=159$, ●:$N=319$, ○:$N=639$, – – :model calculation, —— :SAW; maximum error in $\langle\cos^2\alpha\rangle$ increases from 0.03 for $N=39$ to 0.05 for $N=639$.

cuss these results in more detail, the orientation functions will be considered first.

Figures 5–7 show $\langle\cos^2\alpha\rangle$, $\langle\cos^2\beta\rangle$ and $\langle\cos^2\gamma\rangle$ as a function of Δ. The symbols and solid lines correspond to the simulation results. The broken lines represent the results of model calculations, which will be discussed in some detail further on. First, the Monte Carlo data will be considered. Figure 5 shows that the orientation function of the longest principal component starts to deviate clearly from the isotropic value of 1/3 for $\Delta\leqslant 2.5$. Hence, the coil starts to align long before any substantial deformation takes place (compare with Fig. 2). Now, the distribution of the centers of mass of all possible conformations is peaked at the center of the slit. Therefore, a range of Δ-values exists for which the longest principal component aligns, but for which there is, on the average, no severe restriction on the orientation of the other two components. Since,

$$\langle\cos^2\alpha\rangle+\langle\cos^2\beta\rangle+\langle\cos^2\gamma\rangle=1 \qquad (6)$$

initially, the decrease in value of the orientation function $\langle\cos^2\alpha\rangle$ is accompanied by an increase in the value of the other two. If Δ is reduced further, the second largest principal component also starts to orient. Figure 6 shows that the corresponding orientation function $\langle\cos^2\beta\rangle$ drops below the isotropic value for $\Delta\leqslant 1$. Obviously, as demonstrated in Fig. 7, $\langle\cos^2\gamma\rangle\to 1$ for $\Delta\to 0$, whereas the other two orientation functions go to zero in this limit.

Although there is a considerable scatter in the data due to statistical errors, Figs. 1–7 clearly demonstrate a universal behavior as a function of Δ for all SAW's considered. Remarkably enough, this corresponding state behavior is valid over the entire Δ-range, including the limit $\Delta\to 0$.

The results presented so far provide ample evidence for the statement that the primary effect of confinement on flexible polymers in a dilute good solvent is to align rather than to deform the coil. Now, these results will be compared with the exact results of an analytic model. In the foregoing, the mean-square principal radii of gyration were used to characterize the average shape of the polymer coil. But more appropriate lengths, as far as the interaction between the plates and the coil is concerned, are the so-called spans. The span or extent of a self-avoiding walk in a given direction is defined

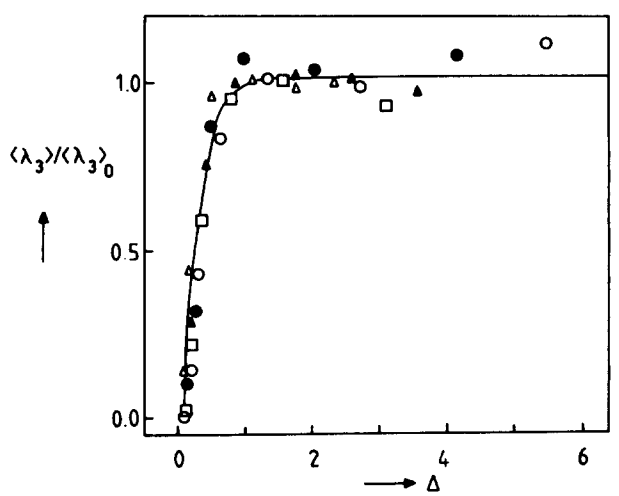

FIG. 4. $\langle\lambda_3\rangle/\langle\lambda_3\rangle_0$ as a function of Δ. ▲:$N=39$, △:$N=79$, □:$N=159$, ●:$N=319$, ○:$N=639$; maximum error is 0.06 for all N.

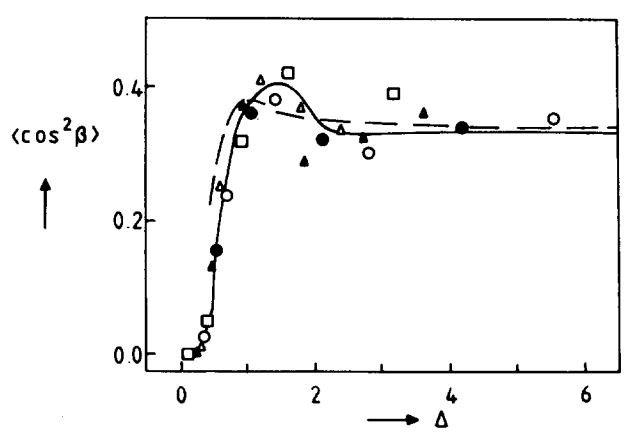

FIG. 6. $\langle\cos^2\beta\rangle$ as a function of Δ. ▲:$N=39$, △:$N=79$, □:$N=159$, ●:$N=319$, ○:$N=639$, – –:model calculation, —— :SAW; maximum error in $\langle\cos^2\beta\rangle$ is 0.05 for all N.

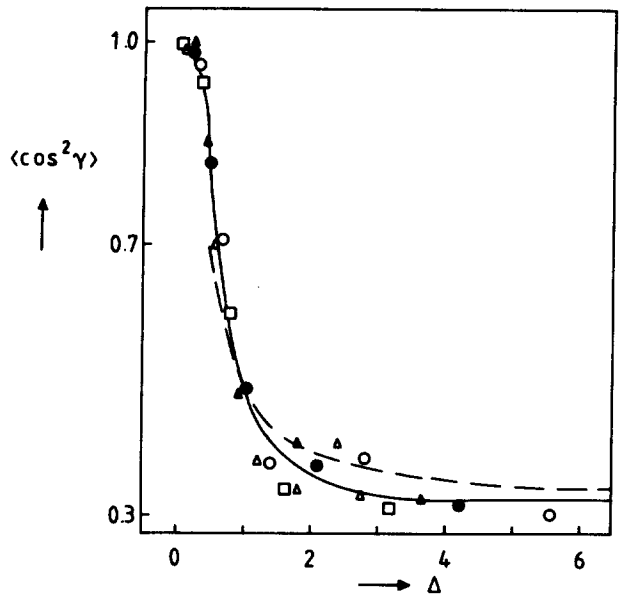

FIG. 7. $\langle \cos^2 \gamma \rangle$ as a function of Δ. ▲:$N = 39$, △:$N = 79$, □:$N = 159$, ●:$N = 319$, ○:$N = 639$, – – :model calculation, —— :SAW; maximum error in $\langle \cos^2 \gamma \rangle$ is 0.065 for all N.

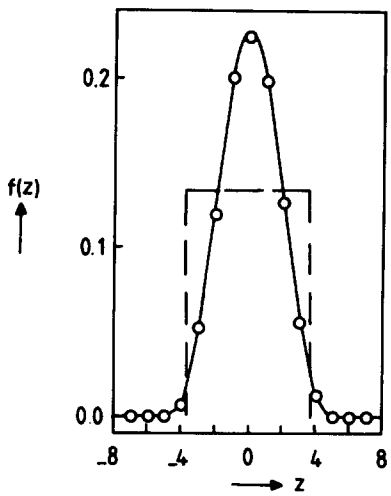

FIG. 8. Center of mass distribution $f(z)$ for all $L = 16$. z:coordinate of the center of mass, – – :model calculation, —— :SAW with $N = 150$; error increases from less than 0.0004 for $|z| > 5$ to 0.02 for $|z| = 0$.

as the minimum distance between two parallel planes normal to the direction between which all occupied lattice sites are located. Different values for the spans are obtained for different sets of orthogonal axes. For a comparison with the results of our simulations, the spans defined for the three orthogonal directions of the principal components of the radius of gyration tensor seem most appropriate. The average values of the corresponding spans will be denoted by s_1, s_2, and s_3. Our model calculation is based on the known results for SAW's of 150 steps on a simple cubic lattice. For this particular case Rubin and Mazur[27] reported

$$s_1 = 24.373, \quad s_2 = 12.892, \quad \text{and} \quad s_3 = 8.553. \tag{7}$$

For comparison, the values of $2\lambda_i^{1/2}$; $i = 1, 2, 3$, are given by

$$2\lambda_1^{1/2} = 14.486, \quad 2\lambda_2^{1/2} = 6.582, \quad 2\lambda_3^{1/2} = 3.763. \tag{8}$$

To obtain a tractable model, we now assume that in first approximation a SAW can be considered as a solid body of an ellipsoidal shape with principal axes a, b, and c ($a \geqslant b \geqslant c$) equal in length to the spans of the SAW along the three orthogonal directions associated with the principal components of the radius of gyration tensor. The explicit calculations will be based on a SAW of length $N = 150$, with a, b, and c given by s_1, s_2, and s_3 of Eq. (7). Making the reasonable assumption that the span lengths scale with N like the radius of gyration [Eq. (2)], the results expressed as a function of Δ are equally valid for all other chain lengths. The details of the model can be found in the Appendix, but here two important points will be mentioned. First, because we are dealing with a solid body, meaningful results can only be obtained for a slit width exceeding c. In terms of the scaled length Δ, this implies

$$\Delta \geqslant c/N^{0.592}. \tag{9}$$

Secondly, we assume that the center of mass of the rigid body can be anywhere between the plates with the same probability, providing its distance to each plate is at least $c/2$. In reality, the distribution of the center of mass of a SAW in a slit is peaked at the center between the plates and only becomes zero at the plates.[28] The assumption of equal probability was made because of its simplicity. Figure 8 illustrates both distributions.

The results of the analytical calculations are shown in Figs. 5–7 by the broken lines. Given the approximations involved, the agreement is quite satisfactory.

APPENDIX

The orientation of an ellipsoidal solid body is studied as a function of the distance ξ of its center of mass from a rigid wall. As far as the interaction with the wall is concerned, only the interaction between the skeleton formed by the three orthogonal axes of length a, b, and c, and the wall will be taken into account. All orientations for which none of the diagonals crosses the wall are assumed to have equal probability. The orientation functions $\langle \cos^2 \alpha \rangle$, $\langle \cos^2 \beta \rangle$, and $\langle \cos^2 \gamma \rangle$ for the angles α, β, γ with the space-fixed axis perpendicular to the wall, of the three diagonal vectors **a**, **b**, and **c**, of length a, b, and c, are evaluated for $c/2 \leqslant \xi$. The problem is formulated in Eulerian angles, being the easiest way to implement integration boundaries of the integrals involved. The coordinates X, Y, and Z of a point P in the space-fixed coordinate system can be represented as a linear function of the coordinates X', Y', and Z' of P in the body-fixed system. The choice of Eulerian angles is according to the X-convention[29]

$$\begin{pmatrix} X \\ Y \\ Z \end{pmatrix} = \mathbf{M} \begin{pmatrix} X' \\ Y' \\ Z' \end{pmatrix}. \tag{A1}$$

The matrix **M** expressed in Eulerian angles is

$$\mathbf{M}=\begin{pmatrix}\cos\psi\cos\phi-\cos\theta\sin\phi\sin\psi & -\sin\psi\cos\phi-\cos\theta\sin\phi\cos\psi & \sin\theta\sin\phi\\ \cos\psi\sin\phi+\cos\theta\cos\phi\sin\psi & -\sin\psi\sin\phi+\cos\theta\cos\phi\cos\psi & -\sin\theta\sin\phi\\ \sin\theta\sin\psi & \sin\theta\cos\psi & \cos\theta\end{pmatrix}.$$

The **a**, **b**, and **c** diagonals of the solid body are identified with the Z', X', and Y' axis. The cosines of the angles between the diagonals and the Z-direction are, according to Eq. (A2), given by

$$\cos\alpha=\cos\theta, \tag{A3}$$

$$\cos\beta=\sin\theta\sin\psi, \quad \text{and} \tag{A4}$$

$$\cos\gamma=\sin\theta\cos\psi. \tag{A5}$$

The differential solid angle, $d\tau$, in terms of Eulerian angles is[30]

$$d\tau=\sin\theta\,d\theta\,d\phi\,d\psi. \tag{A6}$$

The integrations performed are for the normalization constant D

$$D=\int_{l_\theta}^{u_\theta}\int_{l_\phi}^{u_\phi}\int_{l_\psi}^{u_\psi}\sin\theta\,d\theta d\phi d\psi \tag{A7}$$

and for the averages

$$\langle\cos^2\alpha\rangle=D^{-1}\int_{l_\theta}^{u_\theta}\int_{l_\phi}^{u_\phi}\int_{l_\psi}^{u_\psi}\cos^2\theta\sin\theta\,d\theta d\phi d\psi, \tag{A8}$$

$$\langle\cos^2\beta\rangle=D^{-1}\int_{l_\theta}^{u_\theta}\int_{l_\phi}^{u_\phi}\int_{l_\psi}^{u_\psi}\sin^3\theta\sin^2\psi\,d\theta d\phi d\psi, \tag{A9}$$

and

$$\langle\cos^2\gamma\rangle=D^{-1}\int_{l_\theta}^{u_\theta}\int_{l_\phi}^{u_\phi}\int_{l_\psi}^{u_\psi}\sin^3\theta\cos^2\psi\,d\theta d\phi d\psi. \tag{A10}$$

The upper and lower integration boundaries are u_i and l_i, where index i is the Euler angle of interest. Because of the orthogonality of the diagonals, the average of one of the cosines can always be calculated from the other two by

$$\langle\cos^2\alpha\rangle+\langle\cos^2\beta\rangle+\langle\cos^2\gamma\rangle=1. \tag{A11}$$

Four different regimes are distinguished depending on the upper and lower integration boundaries.

1) $\xi\geqslant a$, where $0\leqslant\theta\leqslant\pi/2$, $0\leqslant\phi\leqslant\pi/2$, and $0\leqslant\psi\leqslant\pi/2$, giving the trivial result

$$\langle\cos^2\alpha\rangle=\langle\cos^2\beta\rangle=\langle\cos^2\gamma\rangle=1/3. \tag{A12}$$

2) For $b\leqslant\xi\leqslant a$, θ is restricted to values for which $0\leqslant\cos\theta\leqslant\xi/a$. For ϕ and ψ, the integration boundaries are as mentioned before. The result is

$$\langle\cos^2\alpha\rangle=1/3(\xi/a)^2 \quad \text{and} \tag{A13}$$

$$\langle\cos^2\beta\rangle=\langle\cos^2\gamma\rangle=1/2-1/6(\xi/a)^2. \tag{A14}$$

3) For $ab/(a^2+b^2)^{1/2}\leqslant\xi\leqslant b$, θ and ψ are restricted to values for which $0\leqslant\cos\theta\leqslant\xi/a$ and $0\leqslant\sin\theta\sin\psi\leqslant\xi/b$. For ϕ, the integration boundaries are as before. In this case, one finds

$$D=\pi/2\{\xi/a-[1-(\xi/b)^2]^{1/2}\}+\int_{\arcsin(\xi/b)}^{\pi/2}\sin\theta\,d\theta\arcsin[\xi/(b\sin\theta)], \tag{A15}$$

$$\langle\cos^2\alpha\rangle=D^{-1}\pi/6\{(\xi/a)^3-[1-(\xi/b)^2]^{3/2}\}+D^{-1}\int_{\arcsin(\xi/b)}^{\pi/2}\cos^2\theta\sin\theta\,d\theta\times\arcsin[\xi/(a\sin\theta)], \tag{A16}$$

and

$$\langle\cos^2\beta\rangle=D^{-1}\pi/12[(1-\xi/b)^{3/2}-3(1-\xi/b)^{1/2}-(\xi/a)^3+3\xi/a]+D^{-1}1/2\int_{\arcsin(\xi/b)}^{\pi/2}d\theta\{\sin^3\theta\times\arcsin[\xi/(b\sin\theta)]-(\xi/b)\sin^2\theta(1-[\xi/(b\sin\theta)]^2)\}. \tag{A17}$$

The value for $\langle\cos^2\gamma\rangle$ is calculated with Eqs. A11, A16, and A17. The analytical parts of the integrals A15–A17 (the first terms) were calculated for $\arccos(\xi/a)\leqslant\theta\leqslant\arcsin(\xi/b)$. For these particular values of θ, ψ can be chosen freely, i.e., $0\leqslant\psi\leqslant\pi/2$.

4) For $c\leqslant\xi\leqslant ab/(a^2+b^2)^{1/2}$, the restrictions on θ and ψ are the same as for $ab/(a^2+b^2)^{1/2}\leqslant\xi\leqslant b$; however, there are no values of θ for which ψ can be chosen freely. For ϕ, the integration boundaries are as before.

$$D=\int_{\arccos(\xi/a)}^{\pi/2}\sin\theta d\theta\arcsin[\xi/(b\sin\theta)], \tag{A18}$$

$$\langle\cos^2\alpha\rangle=D^{-1}\int_{\arccos(\xi/a)}^{\pi/2}\cos^2\theta\sin\theta\,d\theta\times\arcsin[\xi/(b\sin\theta)], \tag{A19}$$

and

$$\langle\cos^2\beta\rangle=D^{-1}1/2\int_{\arccos(\xi/a)}^{\pi/2}d\theta\{\sin^3\theta\times\arcsin[\xi/(b\sin\theta)]-(\xi/b)\sin^2\theta\times(1-[\xi/(b\sin\theta)]^2\}. \tag{A20}$$

As mentioned in the main text, the lengths of the diagonals of the solid body were set equal to the value of the spans of a SAW with $N=150$ in the direction of the principal axes: $a=24.373$, $b=12.892$, and $c=8.553$.[27]

The orientation functions for the solid body were calculated for a slit. The distribution function f of the center of mass in the slit was chosen to satisfy:

$$\int_{-L/2}^{L/2}f(z)dz=1,$$

$$f(z)=1/(L-c) \quad |z|\leqslant L/2-c/2,$$

and

$$f(z) = 0 \quad |z| > L/2 - c/2 . \tag{A21}$$

Here, z is the coordinate of the center of mass in the space-fixed coordinate system, whereby for $z = 0$, the center of mass is in the symmetry plane of the slit.

[1] W. Kuhn, Kolloid Z. Polym. **68**, 2 (1934).
[2] K. Šolc, and W. H. Stockmayer, J. Chem. Phys. **54**, 2756 (1971).
[3] K. Šolc, J. Chem. Phys. **55**, 335 (1971).
[4] K. Šolc, Polym. News **4**, 67 (1977).
[5] B. E. Eichinger, Macromolecules **10**, 671 (1977).
[6] B. E. Eichinger, Macromolecules **18**, 211 (1985).
[7] G. Wei, and B. E. Eichinger, Macromolecules **22**, 3429 (1989).
[8] J. Mazur, C. M. Gutman, and F. L. McCrackin, Macromolecules **6**, 872 (1973).
[9] F. H. Abernathy, J. R. Bertschy, and R. W. Chin, J. Rheology **24**, 647 (1980).
[10] W. Gobush, K. Šolc, and W. H. Stockmayer, J. Chem. Phys. **60**, 12 (1974).
[11] F. Brochard, J. Polym. Sci., Polym. Phys. Ed. **17**, 1367 (1979).
[12] H. Mattoussi and M. Veyssie, J. Physique **50**, 99 (1989).
[13] J. H. van Vliet and G. ten Brinke, (in preparation).
[14] D. E. Kranbuehl and P. H. Verdier, J. Chem. Phys. **56**, 3145 (1972).
[15] D. E. Kranbuehl and P. H. Verdier, J. Chem. Phys. **67**, 361 (1977).
[16] F. T. Wall, F. Mandel, and J. C. Chin, J. Chem. Phys. **65**, 2231 (1976).
[17] F. T. Wall, J. C. Chin, and F. Mandel, J. Chem. Phys. **66**, 3066 (1977).
[18] F. T. Wall, W. A. Seitz, J. C. Chin, and F. Mandel, J. Chem. Phys. **67**, 434 (1977).
[19] F. T. Wall, W. A. Seitz, J. C. Chin, and P. G. de Gennes, Proc. Natl. Acad. Sci. U.S.A. **75**, 2069 (1978).
[20] M. Daoud and P. G. de Gennes, J. Phys. **38**, 85 (1977).
[21] A. K. Kron, Polym. Sci. USSR **7**, 1361 (1965); A. K. Kron, and P. B. Ptitsyn, Polym. Sci. USSR **9**, 847 (1967); A. K. Kron, O. B. Ptitsyn, and A. J. Skvortsov, Molec. Biol. **1**, 487 (1967).
[22] F. T. Wall and F. Mandel, J. Chem. Phys. **63**, 4592 (1975); F. Mandel, J. Chem. Phys. **70**, 3934 (1979).
[23] P. Flory, *Principles of Polymer Chemistry*, Chap. XII (Cornell University, Ithaca, NY, 1972).
[24] P. G. de Gennes, *Scaling Concepts in Polymer Physics* (Cornell University, Ithaca, NY 1985).
[25] D. C. Rapaport, J. Phys. A **18**, 113 (1985).
[26] N. Madras and A. D. Sokal, J. Stat. Phys. **50**, 109 (1988).
[27] R. J. Rubin and J. Mazur, Macromolecules **10**, 139 (1977).
[28] A. T. Clark and M. Lal, J. Chem. Soc. Faraday Trans. **77**, 981 (1981).
[29] H. Goldstein, *Classical Mechanics* (Addison-Wesley, Reading, 1980).
[30] R. E. Miles, Biometrika **52**, 636 (1965).